ACES Asian Chemical Editorial Society

DOI: 10.1002/asia.201701277

CHEMISTRY AN ASIAN JOURNAL Full Paper

Pyrazines

Click Chemistry Derived Pyridazines: Electron-Deficient Building Blocks with Defined Conformation and Packing Structure

Irén Birkenfelder, Johannes Gurke, Lutz Grubert, Stefan Hecht,* and Bernd M. Schmidt*[a]

Abstract: A series of 3,6-bis(4-triazolyl)pyridazines equipped with terminal phenyl substituents with varying degree of fluorination were synthesized by using the facile copper-catalyzed azide–alkyne cycloaddition and their structures were thoroughly investigated in the gas phase, in solution, and in the solid state by employing DFT calculations, NMR spectroscopy, and single-crystal X-ray diffraction, respectively. On the molecular level, their structure is governed by the strong preference of the triazole-pyridazine linkages for the *anti*-conformation. The supramolecular organization of the molecules in the crystalline solid is controlled by π-stacking, C–H···π as well as C–F···H interactions. The latter can conveniently be tuned by the number and position of fluorine substituents in the terminal phenyl units, giving rise to either herringbone-like, 1D or 2D lamellar packing. Electrochemistry and optical spectroscopy of all compounds suggest that they might find use as electron-transporting/hole-blocking materials in organic electronics.

Introduction

The Cu-catalyzed azide-alkyne cycloaddition reaction (CuAAC)[1] with its oftentimes virtually quantitative yields and exclusive regioselectivity when compared to the uncatalyzed 1,3-dipolar cycloaddition as pioneered by Huisgen[2] quickly advanced to one of the most useful reactions available. This specific transformation's exceptional utility is documented by the fact that despite its rather recent discovery it has been employed across fields, including bioorganic chemistry,[3a,b] organic[3c] and material synthesis[3d] as well as polymer science[3e] and supramolecular chemistry.[3f,g] The generated 1,2,3-triazole ring is furthermore a suitable ligand in organometallic coordination chemistry[3h] and has attracted considerable attention in homogeneous catalysis.[4] Even in the absence of coordinating metal ions, triazole-containing building blocks are able to display well-defined conformational preferences,[4] which can be used to replace amide bonds in peptidomimetics,[5] or to design (hetero)-aromatic foldamers.[6] For the latter, we were originally interested in triazole-derived motifs with defined kinks and explored in particular pyridine[7] but also properly *ortho*-substituted phenyl moieties.[8] In these designs, we took advantage of the high preference for the *anti,anti*-conformation about the C–C bond connecting the triazolyl and (het)aryl units as illustrated for the case of 2,6-bis(1-aryl-1,2,3-triazol-4-yl)pyridines (BTPs) in Scheme 1, left.[9] However, in these designs the generated kinks are substantial and lead to helical foldamers with limited diameter and hence little potential for binding of larger organic guests in their interior.[10] Thus, we became interested in extended motifs with more subtle curvature in order to construct helices with larger inner diameter. Utilizing the same attractive two-fold H-bonding interactions between the acidic triazole H-atom and the neighboring *ortho*-*N*-atom as well as the *ortho*-H-atom and the triazole-N(3)-atom—and thereby avoiding the strongly repulsive *N*-*N*-interactions in the disfavored *syn,syn*-conformation—we introduced a central pyridazine unit to generate 3,6-bis(4-triazolyl)pyridazines (BTPNs, see Scheme 1, right).[11] The BTPNs should display a much wider angle and in addition, due to their large extent of nitrogen incorporation, exhibit strong electron-accepting properties, potentially interesting for electron-transporting/hole-blocking materials.

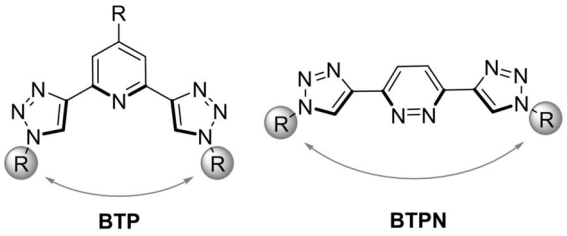

Scheme 1. Triazole-containing kinked structural motifs 2,6-bis(1-aryl-1,2,3-triazol-4-yl)pyridine (BTP) and 3,6-bis(4-triazolyl)pyridazines (BTPN) in their predominantly populated *anti,anti*-conformation.

Herein we present a systematic investigation of BTPNs, in particular focusing on a series of fluorinated derivatives to fur-

[a] *I. Birkenfelder, J. Gurke, Dr. L. Grubert, Prof. S. Hecht, Dr. B. M. Schmidt*
Department of Chemistry and IRIS Adlershof, Humboldt-Universität zu Berlin, Brook-Taylor-Str. 2, 12489 Berlin (Germany)
E-mail: sh@chemie.hu-berlin.de
bernd.schmidt@hu-berlin.de

Supporting information and the ORCID identification number(s) for the author(s) of this article can be found under https://doi.org/10.1002/asia.201701277.

ther increase their acceptor strength and modulate their packing behavior. We studied their structure on the molecular level with regard to backbone conformation, both in solution as well as in the crystalline solid and compared our experimental with computational results. With the aid of single-crystal X-ray diffraction, we were able to decipher packing interactions, which are critical for the compounds' electronic properties in the bulk. In addition, we investigated their optoelectronic properties, that is, their ability to act as suitable electron-acceptors while maintaining their optical gap and remaining transparent in the visible region of the spectrum.

Results and Discussion

To maximize the modularity of the system, 3,6-ethynylpyridazine (**1**) was envisioned to be coupled with the respective azides (**2a–h**) by employing CuAAC to yield the desired functionalized 3,6-bis(1-aryl-1*H*-1,2,3-triazol-4-yl)pyridazines (**3a–h,** Scheme 2). The selected core unit **1** was synthesized starting

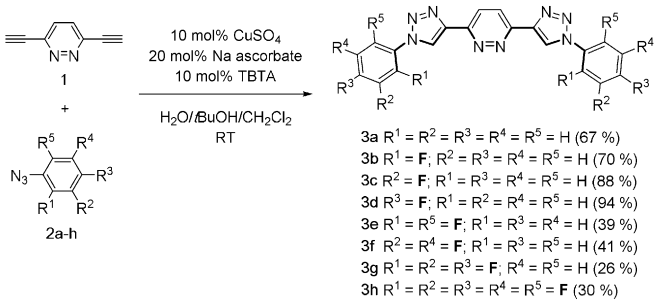

Scheme 2. Synthesis of 3,6-bis(1-aryl-1*H*-1,2,3-triazol-4-yl)pyridazines **3a–h** by CuAAC (TBTA = tris(benzyltriazolylmethyl)amine). Yields are calculated based on the conversion of 3,6-ethynylpyridazine **1.**

from commercially available 3,6-dichloropyridazine by Pd-catalyzed ethynylation,[12] giving the protected 3,6-bisethynylpyridazine (**4**) in high yield. Deprotection of tri(iso-propyl)silyl-protected **4** was quantitative but due to the high reactivity of the building block, it was used immediately in the subsequent reactions and never stored. While azides **2a–g** can conveniently be synthesized by standard diazotization,[13] pentafluorophenylazide **2h** tends to form explosive polyazides upon diazotization.[14] Because of their volatility, prepared azides were not dried excessively but used in slight excess while still containing residual solvent.

To create helically folded backbones and generate materials with potentially high electron mobilities, facile rotation about sigma bonds leading to twisted (hetero)aromatics is not desirable. In compounds **3a–h**, the torsion angles (φ) connecting the central pyridazine and neighboring triazole units (C(pyridazyl)-C(triazolyl) axis) should display characteristic minima and the BTPN core is expected to strongly favor the *anti*-conformation (Scheme 3). The second pair of torsion angles (ν) between the interior triazoles and terminal phenyl units should also display a conformational bias, in particular in case of *ortho*-fluorine substitution.[8]

To confirm these conformational preferences for the BTPN series, solution NMR studies using the nuclear Overhauser effect (NOE) were performed. If the *anti,anti-conformation* shown in Scheme 3 left dominates, no NOE peak can be observed for the protons H1/H2 and H1/H3. Unfortunately protons H3 and H6 show overlapping multiplets in the ^{1}H NMR in DMSO[D_6], hampering quantitative assessment of NOE signals (Figure S1–2 in the SI). The rotation around the C(pyridazyl)-C(triazolyl) axis (torsion angle φ) is hindered and accordingly, **3b** predominantly populates the *anti*-conformation in DMSO[D_6] solution, as shown in Scheme 3. For a qualitative direct comparison, the NOE spectrum of **3c** (Figure S2) shows strong NOE signals for the protons H1/H3 and H1/H6 because fast rotation around the *N*-C(aryl) axis (angle ν) can be assumed. In contrast, this is not the case for **3b**, in which the neighboring C–F···H interaction favors the *anti*-conformation, resulting in very weak NOE signals (Figure 1).

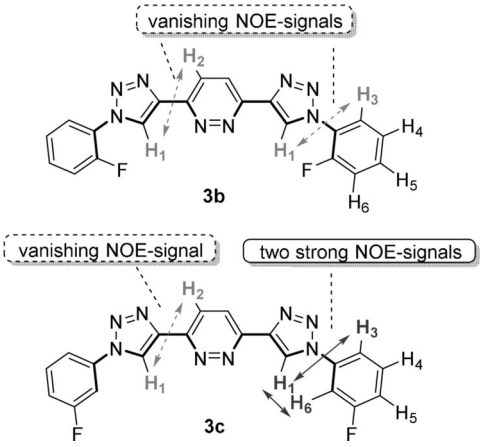

Figure 1. Observed NOE signals for key compounds **3b** and **3c**.

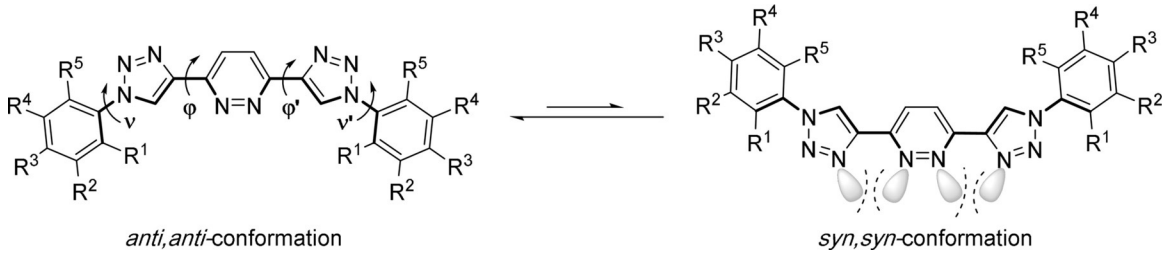

Scheme 3. Conformational preferences of BTPNs: Torsion angles φ and ν are defined by the twist of the triazole plane with regard to the plane of the central pyridazine and terminal phenyl units, respectively.

Computational studies. All structures were investigated by DFT calculations at HSEh1PBE/6–31+G(d,p) level of theory[15] to elucidate the presented system comprehensively (see Table S1 in the SI for angles and bond lengths of **3a**–**3h**). The rotational energy barrier for the rotation around the C(pyridazyl)-C(triazolyl) axis was exemplarily calculated for **3a**,**b** and **3e** (Figure 2).

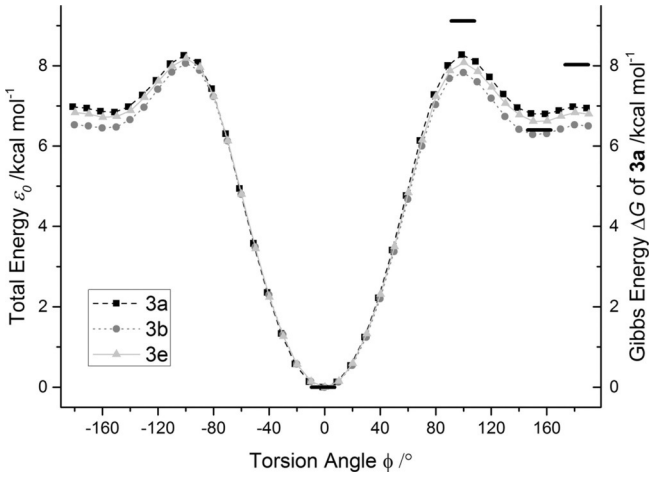

Figure 2. Conformational preference of central BTPN core: Total energy as a function of the rotation around the C(pyridazyl)-C(triazolyl) axis (the torsion angle φ) for key compounds bearing no (**3a**), one (**3b**) or two fluorine substituents (**3e**) in *ortho*-position, respectively. Bars (right axis) indicate the Gibbs energy for the relevant stationary points for **3a**.

As expected, the rotation of the triazole ring with respect to the pyridazine core is largely independent from the potential fluorine substituents in *ortho*-position on the attached phenyl groups. In all cases, the global minimum was found around 0°, corresponding to maximum π-conjugation. Potential steric repulsion in the coplanar geometry is minimized due to the favorable angles of five-membered rings adjacent to six-membered rings (in strong contrast to biphenyl for example).[16] Upon rotation leading to an increasingly twisted system, energy gained from π-conjugation is gradually lost until the perpendicular transition state that connects the global minimum with two local minima. The latter enable π-conjugation but suffer from strongly repulsive interactions between the neighboring *N*-atom's lone pairs as well as the pyridazine and triazole H-atoms. To further quantify the conformational analysis (see also Figure S3), the relevant stationary points on the reaction path around the torsion angle φ, specifically, global and local minima as well as the connecting transition state, were calculated. The computed Gibbs energies verify the previous findings, however underestimate the energy of the transition states and overestimate the energy of the minima. These results clearly verify the predominant *anti*-conformer in the gas phase by DFT calculations.

Subsequently, the rotation around the *N*-C(aryl) axis, described by angle ν, was elucidated by focusing once again on the key compounds for each group (Figure 3). The first group is represented by **3a** and includes all other compounds only

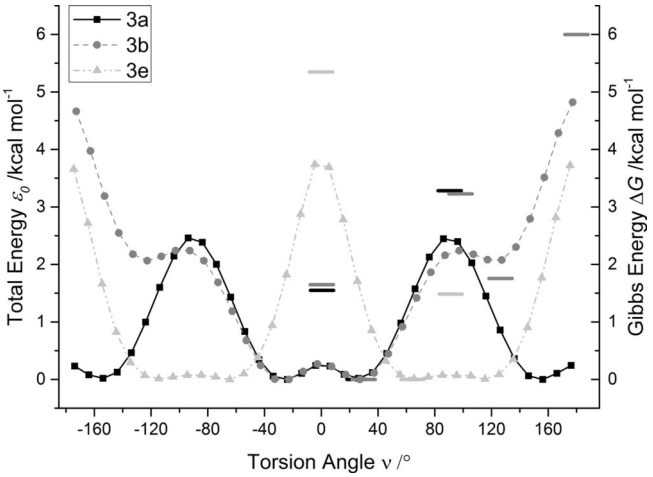

Figure 3. Conformational preference of terminal phenyl units: Total energy as a function of the rotation around the *N*-C(aryl) axis (torsion angle ν) for key compounds bearing no (**3a**), one (**3b**) or two fluorine substituents (**3e**) in *ortho*-position, respectively. Bars (right axis) indicate the Gibbs energy for the relevant stationary points.

bearing protons in *ortho*-position (**3a**, **3c**, **3d** and **3f**). This group is characterized by two local minima of equal energy, avoiding C–H···H-C repulsion by slightly twisting to ca. 25°. The separating barriers originate from rotating towards a 90° perpendicular geometry, where steric hindrance is minimal yet the penalty of lost π-conjugation becomes maximal.

The second group consists of all compounds bearing one F-atom in *ortho*-position (**3b** and **3g**). In line with the first group, the rotation to approximately 0° is unfavorable but in contrast to group one, two global minima exist at around 25° when the steric hindrance induced by the larger fluorine atom is minimal but the possibility of forming an attractive C–F···H interaction is given. When angle ν approaches 90°, again the loss of π-conjugation is responsible for the rise of total energy, leading to local minima at 123°. The largest penalty is observed when the F-atom's and the opposite *N*-atom's lone pairs face each other, which is not even remotely compensated by the gain in π-conjugation. The third group consists of BTPNs bearing two F-atoms in *ortho*-position (**3e** and **3h**). *Ortho*-disubstitution leads to a drastically different overall horseshoe-like shape of the molecules, as the global minima for torsion angle ν are located at about 60°. The loss of π-conjugation seems to be compensated again by the seemingly large steric penalty, also observed in the second group. Overall the F-atoms induce both an attractive C–F···H contact as well as a repulsive interaction between the F- and *N*-atoms, leading to a slightly smaller barrier in comparison to the second group. These computational results for the gas phase are confirmed by experimentally determined solid-state structures (vide infra).

Single crystal X-ray structure analyses. The solid-state structures of six compounds, **3a**–**e** and **3g**, were elucidated by X-ray diffraction of suitable single crystals. All obtained structures are collected in the SI together with selected geometrical parameters (listed in Table S6) and crystallographic details. Again, we focus here on the solid-state structures of key com-

pounds **3a**, **3b**, and **3e** as depicted in Figure 4. While compounds **3a** and **3e** show nearly coplanar geometry at the core, compound **3b** is somewhat twisted ($\nu = 15^\circ$). As expected based on the computation, the *ortho,ortho'*-difluorophenylated derivative **3e** strongly deviates from planarity with regard to the second torsion angle ($\varphi = 51^\circ/45^\circ$). Please note that the observed angle deviations originate either from crystal packing effects or from differences of the structures in each phase, which is difficult to distinguish.

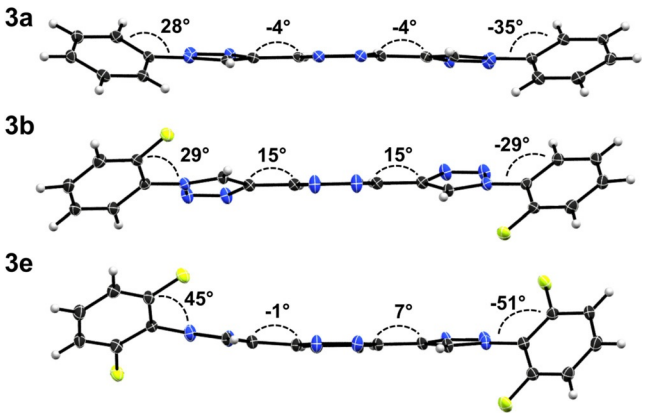

Figure 4. Geometries of the key compounds **3a** (top), **3b** (middle), and **3e** (bottom) as obtained from single-crystal X-ray structure analyses and corresponding torsion angles φ and ν.

With regard to crystal packing, the six pyridazines presented herein display all common solid-state packing motifs (Figure 5), namely herringbone-like packing (**3e**), 1D lamellar packing (**3a**, **3c**, **3d**), and 2D lamellar packing (**3b**, **3g**). Thus deliberately choosing the fluorine-substitution pattern of the terminal phenyl moieties provides full control over the resulting solid-state structure.[17]

The observed supramolecular organization in the crystalline solid is most likely originating from intermolecular C–H···π[18] as well as C–F···H interactions.[19] A common motif observed herein is the interaction of the *N*-atoms of one pyridazine ring with the H-atoms of a neighboring pyridazine ring (ca. 2.52 Å) leading to their coplanar orientation and thus formation of 2D layered arrangements. Compounds **3a**, **3c**, and **3d**, displaying 1D lamellar packing, furthermore engage in close π-stacking of the central pyridazine with triazole rings of adjacent molecules in distances of 3.57 Å and 3.60 Å (centroid-to-centroid distances) and close π-stacking without offset in the case of **3c** (3.60 Å). The structures of **3b** and **3g**, exhibiting 2D lamellar packing, in contrast are largely dominated by C–F···H (2.56–2.73 Å) and C–H···N interactions (2.58–3.01 Å). The same holds true for compound **3e**, which shows a variety of interlayer C-F···H contacts (2.56–3.01 Å) as close π-stacking contacts are not feasible. The unit cell and additional images illustrating the plethora of these intramolecular weak interactions are depicted in the SI (Figure S6–21) and constitute a detailed and comprehensive study of such interactions in this class of heteroaromatic compounds.

Material properties. After having investigated both the intra- as well as intermolecular interactions manifested in conformation as well as packing, we investigated their influence on the optical and electronic properties of all BTPN derivatives (**3a–h**) and their data is summarized in Table 1. No solvatochromism was observed when dissolving **3b** in common organic solvents, such as MeCN, MeOH or DCM. Furthermore, neither fluorescence nor phosphorescence emission was observed. The absorption spectra of **3a–h** (see Figure S4 in the SI) all follow similar features with a maximum hypsochromic shift of 15 nm in **3h** as compared to **3a**. However, since fluorine substitution usually lowers both the HOMO and the LUMO energy level, a strong shift of the band gap is not expected and the changes observed might also correspond to the geometry changes of the molecules upon fluorine substitution, that is, the torsion angles affecting the extent of π-conjugation.

All compounds except **3b** exhibit quasi-reversible and irreversible cyclic voltammetric responses in DMF (see Table 1). Observed reductions occur between −1.9 to −2.0 V in DMF and are largely independent from the fluorine substitution pattern. However, the half potential ($E_{1/2}$) of the reduction of **3h** bearing pentafluorophenyl groups is shifted by 0.1 V towards higher potentials relative to its perhydrogenated analogue **3a**. It should be pointed out that due to the irreversibility, the onset values are difficult to determine, the conservative approximations lead therefore to similar energies for the LUMO of the compounds studied herein (ca. 2.35 eV). Additional cyclic voltammetric data using acetonitrile or THF for molecules, which could sufficiently be dissolved in these solvents, is compiled in the SI (see Figure S5 and Table S4). Although reductions remain irreversible, a clear trend can be observed for

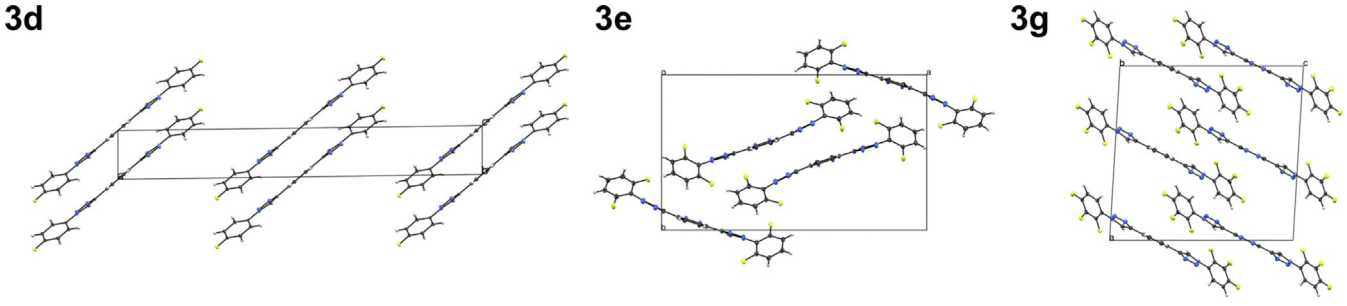

Figure 5. Packing motifs in the crystalline solid involve: 1D lamellar packing for **3d** (left), herringbone-like packing for **3e** (middle), and 2D lamellar packing for **3g** (right).

Table 1. Summary of electronic and optical properties of BTPN derivatives.

	UV/Vis λ_{max} [nm]	Electrochemistry E_p^c in V[SCE] MeCN	E_p^c in V[SCE] DMF	E_{LUMO} in [eV]	DFT HSEh1PBE/6-31+G(d,p)
3a	286	<-2.7	−1.930 (qr)	−2.35	−2.04
3b	279	−2.459	−1.944 (r)	−2.34	−2.10
3c	283	–	−1.925 (qr)	−2.36	−2.22
3d	274	–	−2.000 (qr)	−2.28	−2.15
3e	273	–	−1.931 (i)	−2.35	−2.02
3f	286	–	−1.900 (qr)	−2.38	−2.45
3g	277	−2.287	−2.000 (qr)	−2.28	−2.28
3h	271	−2.145	−1.919 (i)	−2.36	−2.45

Summary of electronic and optical properties. Absorption of the compounds **3a–h** in acetonitrile [c(**3a**) = 4.201×10^{-5} M, c(**3b**) = 3.452×10^{-5} M, c(**3c**) = 1.189×10^{-5} M, c(**3d**) = saturated solution, c(**3e**) = 4.303×10^{-5} M, c(**3f**) = 3.087×10^{-5} M, c(**3g**) = 4.108×10^{-5} M, c(**3h**) = 3.439×10^{-5} M]. Electrochemical cathodic peak potentials, (r) = reversible, (qr) = quasi reversible, (i) = irreversible: $c = 1\times10^{-3}$ mol L^{-1} in 0.1 M Bu_4NPF_6 DMF, Pt-disc d = 1 mm, dE/dt = 1 V s^{-1}, $E_{LUMO} = -e$ ($E^p_{c\ vs.\ Fc/Fc+}$) −4.8 eV.

cyclic voltammetric responses in acetonitrile, where observed reductions shift drastically to lower potential upon fluorine substitution.

Conclusions

By employing a highly modular click synthesis approach we have developed a convenient pathway to synthesize 3,6-bis(4-triazolyl)pyridazines (BTPN) derivatives with defined conformational preferences, which govern their structure in solution and control their packing in the solid state. The highly conserved *anti*-conformation of the central pyridazine core provides access to extended building blocks with wide angles that should allow for the design of foldamer hosts with large interior diameters suitable for host-guest chemistry with large guest molecules.[10,11] Furthermore, the flat molecular geometry in combination with specifically introduced fluorine substituents allows for control over the supramolecular organization in the crystalline solid. In particular in view of the electron-poor character of the BTPN scaffold such exquisite engineering of the packing should prove advantageous to custom tailor these n-type organic semiconductors as electron-transporting/ hole-blocking materials for applications in (opto)electronic devices.

Experimental Section

General information, all experimental procedures, compound characterization data of all new compounds and additional data (UV/vis spectroscopy, calculations, X-ray analyses and electrochemical details) is contained in the supporting information. CCDC 1571320 (**3a**), 1571315 (**3b**), 1571318 (**3c**), 1571319 (**3d**), 1571317 (**3e**), and 1571316 (**3g**) contain the supplementary crystallographic data for this paper. These data can be obtained free of charge from The Cambridge Crystallographic Data Centre.

General procedure for preparation of aromatic azides:[7a] The respective aniline (20.8 mmol, 1 equiv.) was suspended in 400 mL of 17% aqueous HCl at room temperature. Ethanol was added until a clear solution was obtained (usually a ratio of 5:1 (aqueous HCl/EtOH) was necessary). The mixture was cooled to 0 °C. $NaNO_2$ (41.6 mmol, 2 equiv.) was added in small portions (attention, release of toxic gas!) and the reaction mixture was stirred for 15 min at 0 °C. Then NaN_3 (41.6 mmol, 2 equiv.) was added in small portions and the mixture stirred for 1 h at 0 °C. The solution was transferred into a separation funnel, water was added and the aqueous phase was extracted with 150 mL of ethyl acetate or diethyl ether (4×). The combined organic phases were washed with water, aqueous $NaHCO_3$, sat. aqueous $NaHCO_3$ solution, and brine. After drying over $MgSO_4$, careful removal of the solvent using a rotary evaporator (some azides are more volatile than others) gave a yellow oil of the respective azide.

General procedure of the copper catalyzed 1,3-dipolar cycloaddition:[7a] 3,6-Diethynylpyridazine **1** (1 equiv.), the respective aryl azide (3 equiv.), sodium ascorbate (0.2 equiv) and TBTA (0.1 equiv.) were dissolved in a solvent mixture of H_2O/*tert*BuOH/CH_2Cl_2. This mixture was degassed and $CuSO_4$ was added (stock solution, 10 mg $CuSO_4$ per 0.1 mL water) and stirred for one to five days at room temperature in the dark. After the starting material was consumed, as indicated by TLC monitoring (product formation was indicated by a spot on or near the baseline), the mixture was transferred to a centrifuge tube (24 mm OD, 30 mL capacity) and washed with 5 mL of 0.05 M aqueous EDTA solution, water, CH_2Cl_2, CH_3CN, and MeOH (4000 rpm for 10 min). Removing of the solvent in vacuo gave the products as colourless solids in high analytical purities. The reaction was usually run on a mmol scale.

Acknowledgements

The authors thank Dr. B. Ziemer (HU Berlin) for carrying out the initial single-crystal X-ray measurements. B.M.S. thanks the Alexander von Humboldt Foundation for continuous support. Generous support by the German Research Foundation (DFG via SFB951) is gratefully acknowledged.

Conflict of interest

The authors declare no conflict of interest.

Keywords: click chemistry · conformation analysis · fluorine · pyridazine · triazole

[1] a) C. W. Tornøe, C. Christensen, M. Meldal, *J. Org. Chem.* **2002**, *67*, 3057–3064; b) V. V. Rostovtsev, L. G. Green, V. V. Fokin, K. B. Sharpless, *Angew. Chem. Int. Ed.* **2002**, *41*, 2596–2599; *Angew. Chem.* **2002**, *114*, 2708–2711.

[2] a) A. Michael, *J. Prakt. Chem.* **1893**, *48*, 94–95; b) R. Huisgen, R. Knorr, L. Möbius, G. Szeimies, *Chem. Ber.* **1965**, *98*, 4014–4021.

[3] a) V. K. Tiwari, B. B. Mishra, K. B. Mishra, N. Mishra, A. S. Singh, X. Chen, *Chem. Rev.* **2016**, *116*, 3086–3240; b) C. S. McKay, M. G. Finn, *Chem. Biol.* **2014**, *21*, 1075–1101; c) V. D. Bock, H. Hiemstra, J. H. Van Maarseveen, *Eur. J. Org. Chem.* **2006**, 51–68; d) W. Xi, T. F. Scott, C. J. Kloxin, C. N. Bowman, *Adv. Funct. Mater.* **2014**, *24*, 2572–2590; e) A. Qin, J. W. Lam, B. Z. Tang, *Chem. Soc. Rev.* **2010**, *39*, 2522–2544; f) Y. Li, M. Pink, J. A. Karty, A. H. Flood, *J. Am. Chem. Soc.* **2008**, *130*, 17293–17295; g) Y. Hua, A. Flood, *Chem. Soc. Rev.* **2010**, *39*, 1262–1271; h) B. Schulze, U. S. Schubert, *Chem. Soc. Rev.* **2014**, *43*, 2522–2571.

[4] a) D. Schweinfurth, L. Hettmanczyk, L. Suntrup, B. Sarkar, *Z. Anorg. Allg. Chem.* **2017**, *643*, 554–584; b) S. Hohloch, D. Schweinfurth, M. G.

Sommer, F. Weisser, N. Deibel, F. Ehret, B. Sarkar, *Dalton Trans.* **2014**, *43*, 4437 – 4450; c) D. Schweinfurth, S. Demeshko, S. Hohloch, M. Steinmetz, J. G. Brandenburg, S. Dechert, F. Meyer, S. Grimme, B. Sarkar, *Inorg. Chem.* **2014**, *53*, 8203 – 8212; d) R. Maity, S. Hohloch, M. van der Meer, B. Sarkar, *Chem. Eur. J.* **2014**, *20*, 9952 – 9961; e) S. Hohloch, C.-Y. Su, B. Sarkar, *Eur. J. Inorg. Chem.* **2011**, 3067 – 3075.

[5] a) W. S. Horne, C. A. Olsen, J. M. Beierle, A. Montero, M. R. Ghadiri, *Angew. Chem. Int. Ed.* **2009**, *48*, 4718 – 4724; *Angew. Chem.* **2009**, *121*, 4812 – 4818; b) Y. L. Angell, K. Burgessa, *Chem. Soc. Rev.* **2007**, *36*, 1674 – 1689.

[6] a) E. Yashima, K. Maeda, H. Iida, Y. Furusho, K. Nagai, *Chem. Rev.* **2009**, *109*, 6102 – 6211; b) E. Yashima, N. Ousaka, D. Taura, K. Shimomura, T. Ikai, K. Maeda, *Chem. Rev.* **2016**, *116*, 13752 – 13990.

[7] a) R. M. Meudtner, S. Hecht, *Angew. Chem. Int. Ed.* **2008**, *47*, 4926 – 4930; *Angew. Chem.* **2008**, *120*, 5004 – 5008; b) R. M. Meudtner, S. Hecht, *Macromol. Rapid Commun.* **2008**, *29*, 347 – 351.

[8] D. Zornik, R. M. Meudtner, T. El Malah, C. M. Thiele, S. Hecht, *Chem. Eur. J.* **2011**, *17*, 1473 – 1484.

[9] It is possible to lock the *syn*,*syn*-conformation of BTPs using metal ions, see: M. Ostermeier, M.-A. Berlin, R. M. Meudtner, S. Demeshko, F. Meyer, C. Limberg, S. Hecht, *Chem. Eur. J.* **2010**, *16*, 10202 – 10213; b) R. M. Meudtner, M. Ostermeier, R. Goddard, C. Limberg, S. Hecht, *Chem. Eur. J.* **2007**, *13*, 9834 – 9840.

[10] a) J. Becerril, J. M. Rodriguez, I. Saraogi, A. D. Hamilton in *Foldamers: Structure Properties and Applications* (Eds.: S. Hecht, I. Huc), Wiley-VCH, Weinheim, **2007**, pp. 195 – 229; b) G. Guichard, I. Huc, *Chem. Commun.* **2011**, *47*, 5933 – 5941.

[11] a) B. Happ, G. M. Pavlov, E. Altuntas, C. Friebe, M. D. Hager, A. Winter, H. Görls, W. Günther, U. S. Schubert, *Chem. Asian J.* **2011**, *6*, 873 – 880; b) S. E. Bodman, C. M. Fitchett, *Dalton Trans.* **2014**, *43*, 12606 – 12613; S. E. Bodman, A. C. Crowther, P. B. Geragthy, C. M. Fitchett, *CrystEngComm* **2015**, *17*, 81 – 89; c) N. Rahanyan, S. Duttwyler, A. Linden, K. K. Baldridge, J. S. Siegel, *Dalton Trans.* **2014**, *43*, 11027 – 11038.

[12] S. Achelle, N. Plé, D. Kreher, F. Mathevet, A. Turck, A.-J. Attias, *Heterocycles* **2008**, *75*, 357 – 374.

[13] E. F. V. Scriven, K. Turnball, *Chem. Rev.* **1988**, *88*, 297.

[14] J. M. Birchall, R. N. Haszeldine, A. R. Parkinson, *J. Chem. Soc.* **1962**, 4966.

[15] The functional of Perdew, Burke and Ernzerhof (PBE) is known for its general applicability and gives usually accurate results for a wide range of systems. Although the Heyd-Scuseria-Ernzerhof (HSE) screened hybrid was designed for solids, the HSE functional provides a reasonably accurate treatment of small and medium-sized molecules while significantly reducing computational effort; B. G. Janesko, T. M. Henderson, G. E. Scuseria, *Phys. Chem. Chem. Phys.* **2009**, *11*, 443 – 454.

[16] J. Jia, H.-S. Wu, Z. Chen, Y. Mo, *Eur. J. Org. Chem.* **2013**, 611 – 616.

[17] a) K. Zhou, H. Dong, H.-L. Zhang, W. Hu, *Phys. Chem. Chem. Phys.* **2014**, *16*, 22448 – 22457; b) B. M. Schmidt, A. K. Meyer, D. Lentz, *CrystEngComm* **2017**, *19*, 1328 – 1333.

[18] M. Nishio, Y. Umezawa, K. Honda, S. Tsuboyama, H. Suezawa, *CrystEngComm* **2009**, *11*, 1757 – 1788; M. Nishio, *CrystEngComm* **2004**, *6*, 130 – 158.

[19] a) R. Fröhlich, T. C. Rosen, O. G. J. Meyer, K. Rissanen, G. Haufe, *J. Mol. Struct.* **2006**, *787*, 50 – 62; b) T. S. Thakur, M. T. Kirchner, D. Bläser, R. Boese, G. R. Desiraju, *CrystEngComm* **2010**, *12*, 2079 – 2085; c) D. Chopra, T. N. Guru, *CrystEngComm* **2011**, *13*, 2175 – 2186; d) J. Shang, N. M. Gallagher, F. Bie, Q. Li, Y. Che, Y. Wang, H. Jiang, *J. Org. Chem.* **2014**, *79*, 5134 – 5144.

Manuscript received: August 30, 2017
Revised manuscript received: October 19, 2017
Accepted manuscript online: October 30, 2017
Version of record online: November 20, 2017